# Spatial clustering of defect luminescence centers in Si-doped low resistivity $Al_{0.82}Ga_{0.18}N$

Gunnar Kusch,[1,a)] M. Nouf-Allehiani,[1] Frank Mehnke,[2] Christian Kuhn,[2] Paul R. Edwards,[1] Tim Wernicke,[2] Arne Knauer,[3] Viola Kueller,[3] G. Naresh-Kumar,[1] Markus Weyers,[3] Michael Kneissl,[2,3] Carol Trager-Cowan,[1] and Robert W. Martin[1]
[1]*Department of Physics, SUPA, University of Strathclyde, Glasgow G4 0NG, United Kingdom*
[2]*Institute of Solid State Physics, Technische Universität Berlin, Hardenbergstr. 36, 10623 Berlin, Germany*
[3]*Ferdinand-Braun-Institut, Leibniz-Institut für Höchstfrequenztechnik, Gustav-Kirchhoff-Str. 4, 12489 Berlin, Germany*

(Received 19 June 2015; accepted 5 August 2015; published online 17 August 2015)

A series of Si-doped AlN-rich AlGaN layers with low resistivities was characterized by a combination of nanoscale imaging techniques. Utilizing the capability of scanning electron microscopy to reliably investigate the same sample area with different techniques, it was possible to determine the effect of doping concentration, defect distribution, and morphology on the luminescence properties of these layers. Cathodoluminescence shows that the dominant defect luminescence depends on the Si-doping concentration. For lower doped samples, the most intense peak was centered between 3.36 eV and 3.39 eV, while an additional, stronger peak appears at 3 eV for the highest doped sample. These peaks were attributed to the $(V_{III}\text{-}O_N)^{2-}$ complex and the $V_{III}^{3-}$ vacancy, respectively. Multimode imaging using cathodoluminescence, secondary electrons, electron channeling contrast, and atomic force microscopy demonstrates that the luminescence intensity of these peaks is not homogeneously distributed but shows a strong dependence on the topography and on the distribution of screw dislocations. © *2015 Author(s). All article content, except where otherwise noted, is licensed under a Creative Commons Attribution 3.0 Unported License.*
[http://dx.doi.org/10.1063/1.4928667]

There are many potential applications for semiconductor devices emitting in the UV spectral region, including: water purification, gas sensing, and medical diagnostics.[1] To realize these multiple-quantum well based UV light emitting devices, high quality $Al_xGa_{1-x}N$ layers are required, the growth of which still presents challenges. One of the main limitations in using $Al_xGa_{1-x}N$ layers with a high AlN content ($x > 80\%$) in devices is inefficient doping. The doping efficiency of high band gap $Al_xGa_{1-x}N$ layers suffers from an increase in the activation energy of the silicon (Si) donor from 12–17 meV in GaN (Ref. 2) up to 238–255 meV in AlN (Refs. 3 and 4), resulting in a lower fraction of active donors, as well as a reduction of the formation energy of compensating and self-compensating defects.[5,6] Carrier trapping at dislocations appears to be another problem since only layers with low dislocation densities show electrically active doping. Understanding these defects is crucial to improving the quality of Si-doped high band gap $Al_xGa_{1-x}N$ layers and devices utilizing these layers. In this paper, we report on the influences of the Si-doping and threading dislocations on the luminescence properties and topography of a series of AlGaN:Si samples.

Obtaining optical information from wide band gap semiconductors is a challenging task. While this has been done using photoluminescence (PL), utilizing 193 nm or 244 nm lasers, the spatial resolution of PL is too low to investigate submicron features. The combination of cathodoluminescence (CL) and secondary electron (SE) imaging in a scanning electron microscope (SEM) enables information to be obtained on the surface morphology and the optical properties at the same time, allowing the two properties to be correlated.[7,8]

In this paper, a series of samples with different levels of Si-doping in the top $Al_{0.82}Ga_{0.18}N$ layer was grown by metalorganic vapour phase epitaxy (MOVPE) on defect reduced AlN buffers.[9] The $SiH_4$/III partial pressure ratio was varied from $1.9 \times 10^{-5}$ (sample A) to $5.9 \times 10^{-5}$ (sample B) and $1.8 \times 10^{-4}$ (sample C), keeping all other growth parameters constant. The variation of the partial pressure resulted in a Si concentration of $3.1 \times 10^{18}\,cm^{-3}$ for sample A, $8.6 \times 10^{18}\,cm^{-3}$ for sample B, and $2.5 \times 10^{19}\,cm^{-3}$ for sample C as determined by wavelength dispersive X-ray spectroscopy (WDX).[10] Details on the growth are given elsewhere.[11]

The thickness of the doped layers was kept constant at $(1570 \pm 50)$ nm. The compositions were determined by high resolution X-ray diffraction (XRD) and WDX to be $(82 \pm 1)$ % AlN. The surface morphology of the samples were investigated using SE imaging and atomic force microscopy (AFM) in contact mode. CL hyperspectral imaging[12,13] was conducted in an environmental SEM with a 125 mm focal length spectrograph with a 600 line/mm grating, 50 $\mu$m slit and cooled charge-coupled device. The samples were tilted by 45° with respect to the incident electron beam, and the generated light is collected by a reflecting objective with its optical axis perpendicular to the electron beam as described by Edwards *et al.*[14] CL measurements were conducted with an acceleration voltage between 5 kV and 15 kV. At these acceleration voltages, 90% of the beam energy is deposited within a depth between 150 nm and 580 nm, respectively, according

a)gunnar.kusch@strath.ac.uk

 © Author(s) 2015

This article is copyrighted as indicated in the article. Reuse of AIP content is subject to the terms at: http://scitation.aip.org/termsconditions. Downloaded to IP: 130.159.24.44 On: Tue, 18 Aug 2015 09:11:29

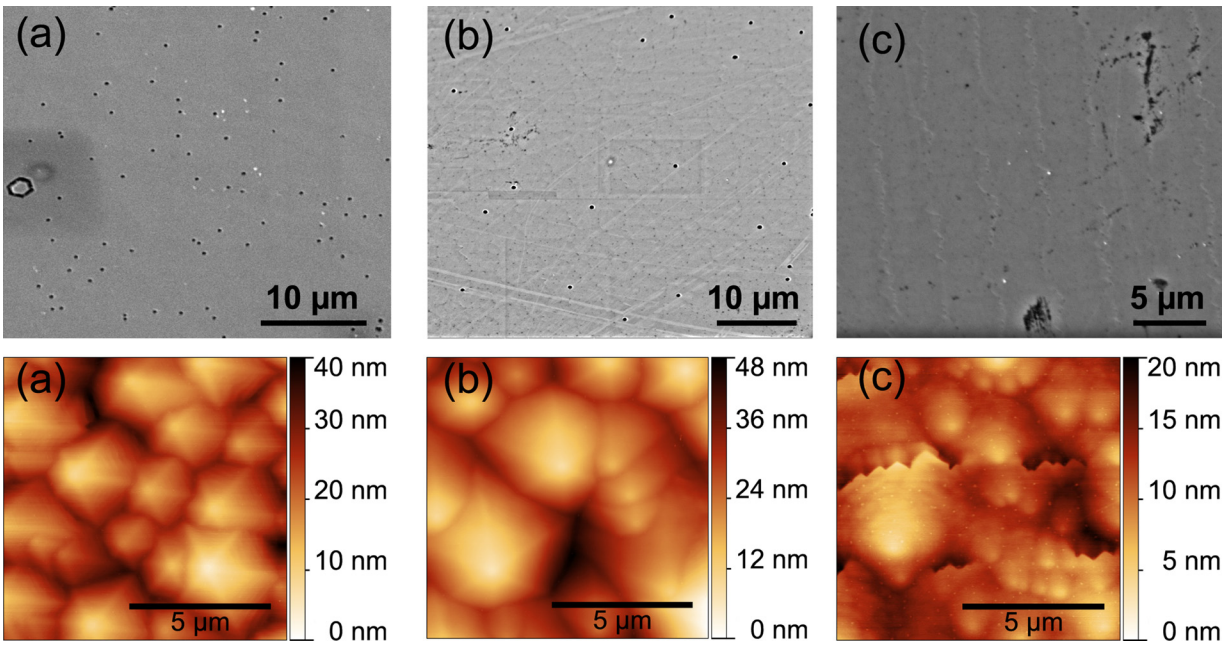


FIG. 1. SE and AFM images of samples A (a), B (b), and C (c).

to Monte Carlo simulations using CASINO software.[15] Electron channeling contrast imaging (ECCI) was performed to investigate the dislocation density, type (e.g., screw/edge), and distribution.[16] ECCI was performed in forescatter geometry where the sample is tilted between 30° and 70° to the incident electron beam and the backscattered detector is placed in front of the sample. The beam current was 2.5 nA, the beam divergence was 4 mrad, and electron beam energy was 30 keV. All measurements were performed at room temperature.

The sheet resistivity was characterised by contactless resistivity measurements and shows that the variation of the $SiH_4$/group-III ratio results in a resistivity of 0.07 Ω cm for sample A, 0.026 Ω cm for sample B, and 0.12 Ω cm for sample C.[11]

SE and AFM images (Fig. 1) reveal that the morphology of samples A and B mainly consists of differently sized hexagonal domains while the morphology of sample C is dominated by step bunches with a periodicity of 3.5 $\mu$m, with hillocks on the terraces between the step bunches. We attribute the change in the surface morphology to a different miscut angle of the underlying substrate. The miscut was specified by the supplier as 0.20° ± 0.15° towards *m*-plane, and within this range, significant variations in topography are possible.[17,18]

The CL spectra for samples A (black line) and B (red dashed) (Fig. 2) consist of three main peaks. Sample A exhibits high energy near band edge (NBE) emission at 5.39 eV and two impurity transitions at 4.35 eV and 3.39 eV, and the measurement additionally shows the second order of the NBE emission. The spectrum for sample B has the NBE emission at 5.32 eV and two impurity transitions at 4.35 eV and 3.36 eV. The CL spectrum for sample C (blue dotted) (Fig. 2) has a NBE emission peak at 5.39 eV and impurity transition at 4.38 eV as well as an additional strong peak at 3 eV. The impurity transition at 3.39 eV observed in the other samples (A and B) is most likely still present but is obscured by the high intensity and large FWHM of this additional peak. The variation in the NBE emission energy between the three samples can be explained by unintentional growth variations, as seen in the WDX measurement, leading to slightly different $Al_xGa_{1-x}N$ compositions as well as a small redshift due to a narrowing of the band gap with increasing Si incorporation as observed by Monroy *et al.*[19] The impurity transition at 4.35 eV is associated with recombination between a shallow donor (Si) and a singly charged deep level acceptor.[20] This singly charged acceptor is attributed to an acceptor complex $(V_{III}–2O_N)^-$. Alternatively, oxygen on an interstitial site ($O_i^-$) would act as a singly charged acceptor.[21] The low energy impurity transition at either 3.39 eV or 3.36 eV is attributed to recombination between a shallow donor (Si) and a doubly charged deep level acceptor. The doubly charged deep level acceptor is most likely an acceptor complex $(V_{III}\text{-}O_N)^{2-}$.[6,22] The redshift in the low energy defect emission (3.36 eV peak) with Si concentration is in good agreement with previous studies by Monroy *et al.*[19] and Nepal *et al.*[20] who attributed it

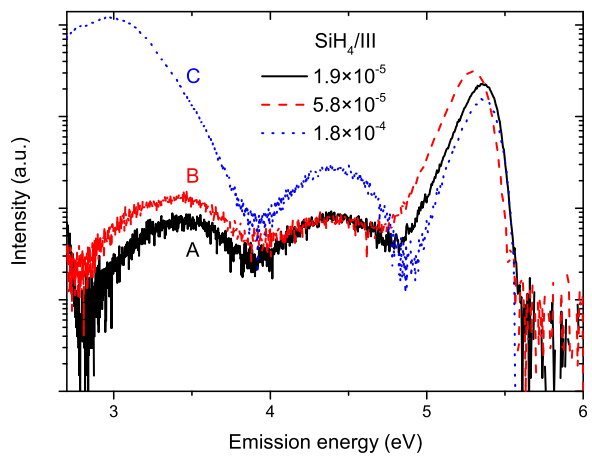


FIG. 2. CL spectra of samples A (black line), B (red dashed), and C (blue dotted).

This article is copyrighted as indicated in the article. Reuse of AIP content is subject to the terms at: http://scitation.aip.org/termsconditions. Downloaded to IP: 130.159.24.44 On: Tue, 18 Aug 2015 09:11:29

to the increasing Si concentration and the variation in the bandgap energy, respectively. The origin of the 3 eV peak is assumed to be recombination between a shallow donor (Si) and a deep acceptor.[22] The deep acceptor is most likely a triply charged cation vacancy $(V_{III})^{3-}$.[6,21] The appearance of the deep acceptor and the increase in resistivity from sample B to sample C, despite an increase in the Si concentration, indicate that for the highest $SiH_4$ flux the sample is in the self-compensating regime.

CL hyperspectral imaging shows that there is a noticeable shift in the energy and intensity of the NBE emission across each sample. Samples A and B show a domain structure (Figs. 3(c) and 3(d)), whereas sample C shows a strong shift in the emission energy along step bunches (not shown). The energy variation in sample C is due to a higher GaN incorporation at the step edges which results in a lower bandgap compared to the surrounding material and explains the increase in the NBE intensity.[18,23] The variation in the emission energy between the different domains in samples A and B could be due to exciton localization at grain boundaries[24] or compositional inhomogeneity.

We have performed SE imaging, CL hyperspectral imaging, and ECCI on the same sample area (Fig. 3) to determine the origin of the observed domain structure. We found that the CL NBE intensity is reduced at the apex of each hillock, while ECCI reveals that a threading dislocation (TD) with a screw component is located at the apex of each hillock (white arrows in Figs. 3(a)–3(c)). The average total TD density for the three samples was estimated to be $1.2 \pm 0.2 \times 10^9\,cm^{-2}$. 3% of the dislocations contain a screw component which is similar to the hillock density. Dislocation type, distribution, and correlation with the hillock morphology will be the subject of a separate paper by Nouf-Allehiani *et al.* As a result, we conclude that the different domains are formed due to spiral growth around a dislocation with a screw component,[25] which acts as a non-radiative recombination center for the NBE emission. The observed difference in the emission energy can be explained by inhomogeneous GaN incorporation. The lowest energy regions are the valleys between the spiral hillocks which provide a high density of steps and kink sites that promote Ga incorporation. The hillocks can exhibit higher levels of GaN incorporation along the surface steps of the spirals again due to the high density of sites for Ga to bond to. In contrast with Ref. 24, we can exclude grain boundaries as the cause of this effect as we do not observe an increased density of dislocations along the edges of the spiral hillocks in these samples.[26]

Fig. 4 shows the backscattered electron (BSE) image and the intensity distribution of the low energy (3.36 eV) CL for sample B. Clear regions with brighter defect luminescence can be observed. Correlation between the CL maps and the corresponding BSE images (one marked with circles in Fig. 4 for better visibility) reveals that the areas of increased defect luminescence intensity are located at and around the apex of each observed hillock. We concluded earlier that the hillocks form due to threading dislocations with a screw component as observed by ECCI.

This indicates that around screw dislocations the formation of compensating defect centers is enhanced. This could be caused by an increased oxygen incorporation around the screw dislocations, as oxygen is known to reduce the formation energy of $V_{Al}$ leading to the formation of the observed $(V_{III}\text{–}2O_N)^-$ and $(V_{III}\text{-}O_N)^{2-}$ complexes or by the core structure of the dislocation itself, which could introduce deep level states in the band gap as calculated by Elsner *et al.*[27] and Belabbas *et al.*[28] for GaN. Different effects could lead to increased oxygen incorporation, namely, the formation of a Cottrell atmosphere[29] or the preferential incorporation of oxygen at the inclined facets surrounding the screw dislocations. The formation of a Cottrell atmosphere is characterized by the drift and diffusion of impurities to a threading dislocation, reducing the strain field surrounding the dislocation. As no correlation between increased oxygen-related defect luminescence and pure edge type threading dislocations is observed, either the interaction energy between the impurities and

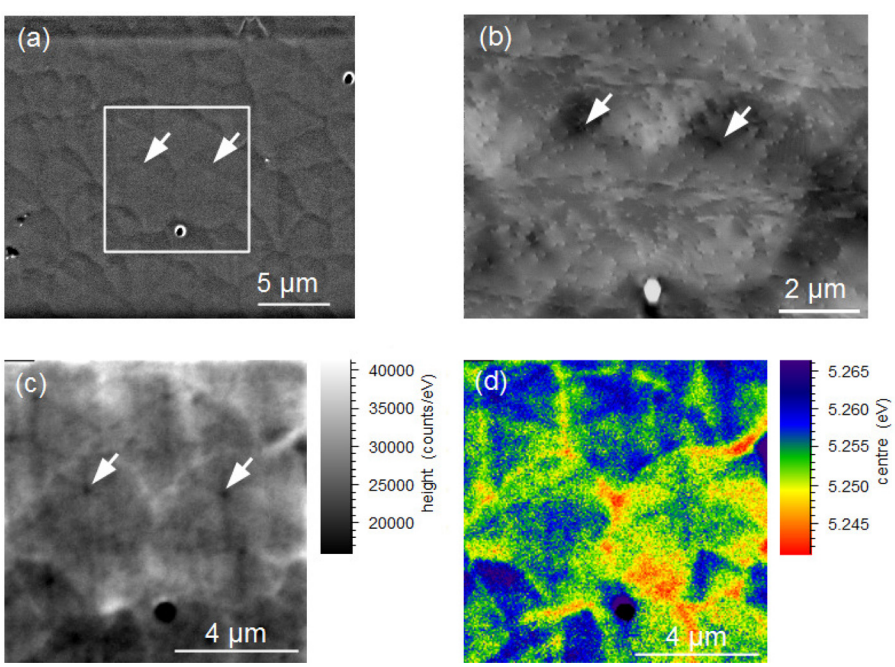


FIG. 3. SE (a) and ECCI image (b) as well as the intensity (c) and energy (d) of the CL NBE peak of sample B.

This article is copyrighted as indicated in the article. Reuse of AIP content is subject to the terms at: http://scitation.aip.org/termsconditions. Downloaded to IP: 130.159.24.44 On: Tue, 18 Aug 2015 09:11:29

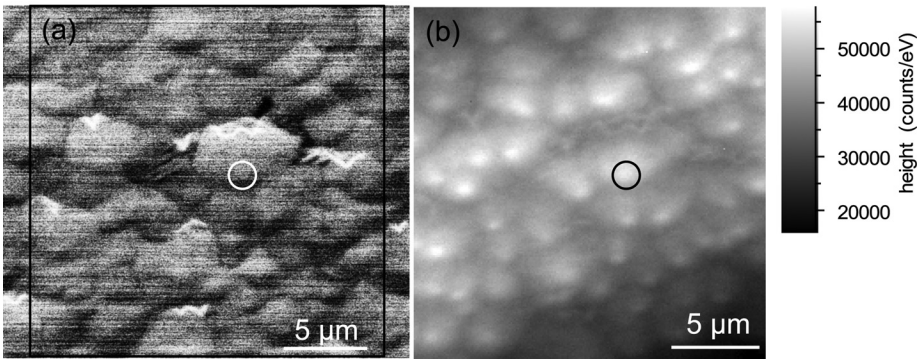


FIG. 4. BSE image (a) and map of the intensity of the 3.36 eV CL peak (b) for sample B.

dislocations with a screw component must be stronger, compared to the interaction with a pure edge dislocation, or the formation of a Cottrell atmosphere is not the reason for the increased oxygen concentration. That no correlation between the pure edge dislocations and the defect luminescence is observed is also in contrast to the calculations by Wright and Furthmüller[30] which predicted that edge dislocations decorated with $V_{Al}$ would have the lowest formation energy of all pure edge dislocations in AlN under nitrogen-rich conditions. Increased oxygen incorporation at different growth facets was observed by Hawkridge and Cherns[31] for open core screw dislocations in GaN and by Herro *et al.*[32] in AlN.

By combining the advantages of CL hyperspectral imaging and ECCI, the influence of threading dislocations on the luminescence properties of $Al_xGa_{1-x}N$:Si was investigated. It was shown that the NBE luminescence is quenched at threading dislocations. The growth of hillocks has been attributed to threading dislocations with a screw component. Additionally, the formation of hillocks leads to an increased defect luminescence intensity around the apices of the hillocks, indicating that both the incorporation of oxygen atoms and the formation of compensating defects are increased. In light of these findings, we assume that the remarkably low resistivities for these samples are partially due to a reduction in the dislocation density as a result of using the epitaxial lateral overgrowth (ELO) $AlN/Al_2O_3$ templates.

We acknowledge funding from the Engineering and Physical Sciences Research Council (EPSRC) (EP/M003132/1) of the UK and German Federal Ministry of Education and Research (BMBF) within the "UltraSens" and "Advanced UV for Life" projects and by the Deutsche Forschungsgemeinschaft (DFG) within the Collaborative Research Center "Semiconductor Nanophotonics" (SFB 787). The data associated with this research are available at http://dx.doi.org/10.15129/9465dccd-6d17-4a84-9d61-8d6fed1c7201 or from the corresponding author.

[1]M. A. Würtele, T. Kolbe, M. Lipsz, A. Külberg, M. Weyers, M. Kneissl, and M. Jekel, Water Res. **45**(3), 1481–1489 (2011).
[2]W. Götz, N. M. Johnson, C. Chen, H. Liu, C. Kuo, and W. Imler, Appl. Phys. Lett. **68**(22), 3144 (1996).
[3]R. Collazo, S. Mita, J. Xie, A. Rice, J. Tweedie, R. Dalmau, and Z. Sitar, Phys. Status Solidi C **8**(7–8), 2031–2033 (2011).
[4]X. T. Trinh, D. Nilsson, I. G. Ivanov, E. Janzén, A. Kakanakova-Georgieva, and N. T. Son, Appl. Phys. Lett. **105**(16), 162106 (2014).
[5]C. G. van de Walle and J. Neugebauer, J. Appl. Phys. **95**, 3851 (2004).
[6]Q. Yan, A. Janotti, M. Scheffler, and C. G. Van de Walle, Appl. Phys. Lett. **105**(11), 111104 (2014).
[7]R. W. Martin, P. R. Edwards, K. P. O'Donnell, M. D. Dawson, C.-W. Jeon, C. Liu, G. R. Rice, and I. M. Watson, Phys. Status Solidi A **201**(4), 665–672 (2004).
[8]G. Naresh-Kumar, J. Bruckbauer, P. R. Edwards, S. Kraeusel, B. Hourahine, R. W. Martin, M. A. Moram, S. Lovelock, R. A. Oliver, C. J. Humphreys, and C. Trager-Cowan, Microsc. Microanal. **20**(1), 55–60 (2014).
[9]A. Knauer, V. Kueller, U. Zeimer, M. Weyers, C. Reich, and M. Kneissl, Phys. Status Solidi A **210**(3), 451–454 (2013).
[10]C. J. Deatcher, K. Bejtka, R. W. Martin, S. Romani, H. Kheyrandish, L. M. Smith, S. A. Rushworth, C. Liu, M. G. Cheong, and I. M. Watson, Semicond. Sci. Technol. **21**(9), 1287 (2006).
[11]F. Mehnke, T. Wernicke, H. Pingel, C. Kuhn, C. Reich, V. Kueller, A. Knauer, M. Lapeyrade, M. Weyers, and M. Kneissl, Appl. Phys. Lett. **103**(21), 212109 (2013).
[12]J. Christen, M. Grundmann, and D. Bimberg, J. Vac. Sci. Technol., B **9**(4), 2358–2368 (1991).
[13]P. R. Edwards, R. W. Martin, K. P. O'Donnell, and I. M. Watson, Phys. Status Solidi C **0**(7), 2474–2477 (2003).
[14]P. R. Edwards, L. K. Jagadamma, J. Bruckbauer, C. Liu, P. Shields, D. Allsopp, T. Wang, and R. W. Martin, Microsc. Microanal. **18**(6), 1212–1219 (2012).
[15]D. Drouin, A. R. Couture, D. Joly, X. Tastet, V. Aimez, and R. Gauvin, Scanning **29**(3), 92–101 (2007).
[16]G. Naresh-Kumar, B. Hourahine, P. R. Edwards, A. P. Day, A. Winkelmann, A. J. Wilkinson, P. J. Parbrook, G. England, and C. Trager-Cowan, Phys. Rev. Lett. **108**, 135503 (2012).
[17]U. Zeimer, V. Kueller, A. Knauer, A. Mogilatenko, M. Weyers, and M. Kneissl, J. Cryst. Growth **377**, 32–36 (2013).
[18]G. Kusch, H. Li, P. R. Edwards, J. Bruckbauer, T. C. Sadler, P. J. Parbrook, and R. W. Martin, Appl. Phys. Lett. **104**(9), 092114 (2014).
[19]E. Monroy, J. Zenneck, G. Cherkashinin, O. Ambacher, M. Hermann, M. Stutzmann, and M. Eickhoff, Appl. Phys. Lett. **88**(7), 071906 (2006).
[20]N. Nepal, M. L. Nakarmi, J. Y. Lin, and H. X. Jiang, Appl. Phys. Lett. **89**(9), 092107 (2006).
[21]D. F. Hevia, C. Stampfl, F. Viñes, and F. Illas, Phys. Rev. B **88**, 085202 (2013).
[22]K. B. Nam, M. L. Nakarmi, J. Y. Lin, and H. X. Jiang, Appl. Phys. Lett. **86**(22), 222108 (2005).
[23]U. Zeimer, A. Mogilatenko, V. Kueller, A. Knauer, and M. Weyers, J. Phys.: Conf. Ser. **471**, 012021 (2013).
[24]I. A. Ajia, P. R. Edwards, Z. Liu, J. C. Yan, R. W. Martin, and I. S. Roqan, Appl. Phys. Lett. **105**(12), 122111 (2014).
[25]B. Heying, E. J. Tarsa, C. R. Elsass, P. Fini, S. P. DenBaars, and J. S. Speck, J. Appl. Phys. **85**(9), 6470–6476 (1999).
[26]W. Qian, M. Skowronski, M. De Graef, K. Doverspike, L. B. Rowland, and D. K. Gaskill, Appl. Phys. Lett. **66**(10), 1252 (1995).
[27]J. Elsner, R. Jones, P. K. Sitch, V. D. Porezag, M. Elstner, Th. Frauenheim, M. I. Heggie, S. Öberg, and P. R. Briddon, Phys. Rev. Lett. **79**(19), 3672–3675 (1997).
[28]I. Belabbas, M. A. Belkhir, Y. H. Lee, J. Chen, A. Béré, P. Ruterana, and G. Nouet, Comput. Mater. Sci. **37**(3), 410–416 (2006).
[29]A. H. Cottrell and B. A. Bilby, Proc. Phys. Soc., London, Sect. A **62**(1), 49–62 (1949).
[30]A. F. Wright and J. Furthmüller, Appl. Phys. Lett. **72**(26), 3467 (1998).
[31]M. E. Hawkridge and D. Cherns, Appl. Phys. Lett. **87**(22), 221903 (2005).
[32]Z. G. Herro, D. Zhuang, R. Schlesser, and Z. Sitar, J. Cryst. Growth **312**(18), 2519–2521 (2010).

This article is copyrighted as indicated in the article. Reuse of AIP content is subject to the terms at: http://scitation.aip.org/termsconditions. Downloaded to IP: 130.159.24.44 On: Tue, 18 Aug 2015 09:11:29